Dalton Transactions

PAPER

Cite this: *Dalton Trans.*, 2017, **46**, 15778

Received 28th September 2017,
Accepted 25th October 2017

DOI: 10.1039/c7dt03649c

rsc.li/dalton

Magnetic properties of $Ln_2CoGe_4O_{12}$ and $LnBCoGe_4O_{12}$ (Ln = Gd, Tb, Dy, Ho, Er; B = Sc, Lu)†

Diming Xu,[a] Maxim Avdeev,[b,c] Peter D. Battle *[a] and D. H. Ryan[d]

Polycrystalline samples of $Ln_2CoGe_4O_{12}$ (Ln = Gd, Tb, Dy, Ho or Er) and $LnBCoGe_4O_{12}$ (B = Sc or Lu) have been prepared and characterised by a combination of magnetometry, ^{155}Gd Mössbauer spectroscopy and, in the case of $Tb_2CoGe_4O_{12}$ and $TbScCoGe_4O_{12}$, neutron diffraction. The holmium- and erbium-containing compositions remain paramagnetic down to 2 K, those containing dysprosium behave as spin glasses and the terbium and gadolinium-containing compounds show long-range magnetic order with transition temperatures below 4 K in all cases. The data can be rationalized qualitatively in terms of the interplay between magnetic anisotropy and crystal field effects.

Introduction

In recent years the family of mixed-metal germanates with the general formula $ABB'Ge_4O_{12}$ has been studied in some detail within the luminescence community.[1–4] A is a relatively-large trivalent or tetravalent cation, often a lanthanide, and B′ is typically a smaller, divalent or trivalent cation from the first long period of the periodic table. B can be a member of either of these two categories provided that the sum of the ionic charges on the three cations is +8. These compounds crystallise in the tetragonal space group *P*4/*nbm*. The cations A occupy the 2*b* site and are coordinated by eight oxide ions at the corners of a square antiprism whereas B and B′ are disordered over a 4*f* site which is at the centre of a distorted octahedron of oxide ions, see Fig. 1. If they are to adopt a disordered arrangement, B and B′ cannot differ greatly in size, and in many cases, for example $ZrMn_2Ge_4O_{12}$,[5] B≡B′. However, in other cases, for example $Y_2CoGe_4O_{12}$,[6] A≡B and compounds, for example $CeMnCoGe_4O_{12}$,[7] containing three different cations are also known.

Our own interest in these germanates centres on their magnetic properties. Many of them have a magnetically-ordered ground state, although the transition from the paramagnetic phase always occurs below 20 K. We have shown previously that $YMnFeGe_4O_{12}$ [8] and compositions in the solid solutions $CeMn_{2-x}Co_xGe_4O_{12}$ [7] and $ZrMn_{2-x}Co_xGe_4O_{12}$ [5] adopt a number of different antiferromagnetic or ferrimagnetic structures and we have been able to identify some of the structural features that determine which structure is adopted in each case. In all of these compounds the strongest magnetic superexchange pathways are of the form (B,B′)–O–Ge–O–(B,B′), that is they pass through tetrahedral GeO_4 groups that link the $(B,B')O_6$ octahedra; the GeO_4 groups themselves share common vertices to form Ge_4O_{12} rings, see Fig. 1. The relatively low magnetic

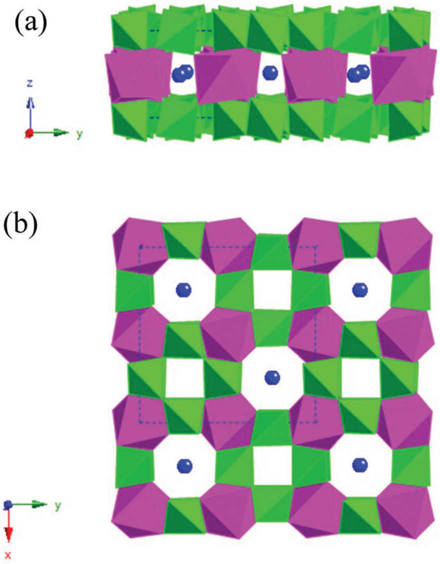

Fig. 1 Crystal structure of $ABB'Ge_4O_{12}$ viewed along (a) [100] and (b) [001]. $B/B'O_6$ octahedra, GeO_4 tetrahedra and A atoms are coloured magenta, green and blue, respectively.

---

[a] Inorganic Chemistry Laboratory, Oxford University, South Parks Road, Oxford, OX1 3QR, UK. E-mail: peter.battle@chem.ox.ac.uk
[b] Australian Nuclear Science and Technology Organisation, Lucas Heights, NSW 2234, Australia
[c] School of Chemistry, The University of Sydney, Sydney, NSW 2006, Australia
[d] Physics Department and Centre for the Physics of Materials, McGill University, 3600 University Street, Montreal, Quebec, H3A 2T8, Canada

† Electronic supplementary information (ESI) available. See DOI: 10.1039/c7dt03649c

transition temperatures are a consequence of the length and complexity of the superexchange pathways. One of the remaining challenges in the study of these compounds is to produce compositions in which all of the cations A, B and B′ take part in the long-range magnetic ordering. Superexchange in these compounds would involve pathways of the form (B,B′)–O–Ge–O–A or (B,B′)–O–A where A is now a magnetic cation. In an attempt to induce the participation of all the cations we have prepared and characterised compositions that can be described by the formulae $Ln_2CoGe_4O_{12}$, wherein A≡B = Ln = Gd^{3+}, Tb^{3+}, Dy^{3+}, Ho^{3+} or Er^{3+} and B′ = Co^{2+}; we have also prepared reference compounds of with the formula $LnBCoGe_4O_{12}$ wherein B is diamagnetic Sc^{3+} or Lu^{3+}. Each composition synthesized in a monophasic form has been characterized by magnetometry and selected samples have been studied in more depth by Mössbauer spectroscopy or neutron diffraction.

Experimental

Polycrystalline samples of the target compositions were prepared using the ceramic method. The appropriate stoichiometric quantities of Co_3O_4, Sc_2O_3, Lu_2O_3 and dried Ln_2O_3 were mixed and ground together with a 5% excess of GeO_2. After an initial heating in powder form at 1075 °C, or 1100 °C in the case of scandium-containing samples, the reaction mixture was pelletised and heated at the same temperature for several days. The mixture was reground and repelleted at least every 48 h. The reaction was deemed to be complete when the X-ray powder-diffraction (XRPD) pattern of the product did not change between successive firings. The XRPD pattern of the final product was recorded at room temperature using a Panalytical X'pert diffractometer operating with monochromated Cu Kα_1 radiation. Data were collected in the range $10 \le 2\theta/° \le 90$ with a step size $\Delta 2\theta = 0.0084°$ and analysed by the Rietveld method[9] as implemented in the GSAS[10,11] program suite.

The magnetic properties of the reaction products were measured with a Quantum Design MPMS 5000 SQUID magnetometer. For each sample the dc magnetic susceptibility was measured in an applied field of 100 Oe over the temperature range $2 \le T/\mathrm{K} \le 300$ after both zero-field-cooling (ZFC) and field-cooling (FC), the field dependence of the magnetization was measured at 2 K over the field range $-50 \le H/\mathrm{kOe} \le 50$ and the ac susceptibility was measured as a function of frequency over the temperature range $2 \le T/\mathrm{K} \le 10$. Additional magnetic measurements were made on samples of particular interest, see below.

Neutron powder-diffraction (NPD) data were collected on $Tb_2CoGe_4O_{12}$ and $TbScCoGe_4O_{12}$ at 300 and 1.5 K on the high-resolution powder diffractometer Echidna at ANSTO. The angular range of $8 \le 2\theta/° \le 160$ was scanned using a step size of $\Delta 2\theta = 0.05°$ with a wavelength of 1.622 Å or 2.4397 Å. The sample was loaded in powder form into a cylindrical vanadium can that was mounted in a cryostat for measurements below room temperature. Angular regions contaminated by scattering from aluminium in the cryostat were excluded from the data analysis. Rietveld analysis of the data was carried out using the peak shape function developed by van Laar and Yelon.[12]

^{155}Gd Mössbauer spectra were collected from samples of $Gd_2CoGe_4O_{12}$, $GdLuGe_4O_{12}$ and $GdScCoGe_4O_{12}$ at temperatures of 5 and 1.8 K. The 50 mCi ^{155}Sm source and sample were mounted vertically in a helium flow cryostat and the Mössbauer drive was operated in sinusoidal mode. The 86.55 keV Mössbauer γ-photons were isolated from the various X-rays emitted by the source with a high-purity Ge detector. The system was calibrated using a laser interferometer with velocities crosschecked against ^{57}Co**Rh**/α-Fe at room temperature and both $^{155}SmPd_3/GdFe_2$ and cubic Gd_2O_3 at 5 K. The ^{155}Gd Mössbauer spectra were fitted using a non-linear least-squares minimization routine with line positions and intensities derived from an exact solution to the full Hamiltonian.[13]

Results

The compositions that were successfully synthesized are listed in Table 1. The X-ray diffraction patterns of all these compounds could be indexed in the tetragonal space group $P4/nbm$; the refined unit-cell parameters, a and c, for each compound are given in the table. A typical fitted X-ray diffraction pattern, that of $Tb_2CoGe_4O_{12}$, is shown in Fig. 2. The eight-coordinate $2b$ sites were found to be occupied by Ln cations in all the $Ln_2CoGe_4O_{12}$ compositions, with the six-coordinate $4f$ sites being occupied by a disordered distribution of Ln and cobalt. Germanium and the two crystallographically-distinct oxygen atoms occupy the $8k$, $8m$ and $16n$ sites with $x_{\mathrm{Ge}} \sim 0.52$ and O1 and O2 close to (−0.37, 0.37, 0.17) and (0.17, 0.06, 0.25), respectively. Four of the compositions studied, $GdLuCoGe_4O_{12}$, $GdScCoGe_4O_{12}$, $TbScCoGe_4O_{12}$, and $DyScCoGe_4O_{12}$ contain two types of trivalent cations. It was not possible to detect any ordering of these cations over the $2b$ and $4f$ sites in $GdLuCoGe_4O_{12}$ by XRPD but in the cases of $GdScCoGe_4O_{12}$ and $TbScCoGe_4O_{12}$ the data indicated that the $2b$ site is occupied by Gd^{3+} or Tb^{3+} and the $4f$ site by Sc^{3+} and Co^{2+}.

For each composition studied, the molar Curie constant, C_{M}, and the Weiss constant, θ, derived by fitting the susceptibility data collected at temperatures above 150 K to the Curie–Weiss law are included in Table 1, as is the temperature, T_{m}, at which any maximum was observed in $\chi(T)$. The Weiss constant is small, that is less than 10 K, and negative for every composition. In order to determine the degree of self-consistency in these data we assumed that intercation interactions are negligible above 150 K and that the spherical Gd^{3+} cations have $S = J = 7/2$. We were then able to calculate a mean Curie constant of 3.63 $m^3\ mol^{-1}$ K for Co^{2+} in the three gadolinium-containing compositions. This is in good agreement with the value of 3.59 determined previously for both $CeCo_2Ge_4O_{12}$ and $ZrCo_2Ge_4O_{12}$. By subtracting this value from the experimentally-determined Curie constants of the other compositions listed in Table 1 we derived values for the effective

Table 1 Unit-cell and magnetic parameters of $Ln_2CoGe_4O_{12}$ and $LnBCoGe_4O_{12}$

Composition	a/Å	c/Å	C_M/cm^3 mol^{-1} K	θ/K	T_m/K	μ_{eff}^{Ln}
$Gd_2CoGe_4O_{12}$	9.9334(1)	4.9562(1)	19.312(1)	−3.43(5)	3.6	—
$Tb_2CoGe_4O_{12}$	9.9028(1)	4.9473(1)	27.034(1)	−8.86(2)	2.8	9.68
$Dy_2CoGe_4O_{12}$	9.8796(1)	4.9412(1)	31.908(1)	−7.77(1)	2.8	10.63
$Ho_2CoGe_4O_{12}$	9.8471(1)	4.9332(1)	31.260(1)	−9.19(2)	—	10.51
$Er_2CoGe_4O_{12}$	9.8271(1)	4.8258(1)	26.518(1)	−6.23(2)	—	9.57
$GdLuCoGe_4O_{12}$	9.8624(1)	4.9236(1)	11.627(1)	−6.09(6)	2.4	—
$GdScCoGe_4O_{12}$	9.8067(1)	4.8392(1)	11.450(2)	−1.67(21)	3.5	—
$TbScCoGe_4O_{12}$	9.7823(1)	4.8356(1)	16.077(2)	−7.37(7)	3.4	9.97
$DyScCoGe_4O_{12}$	9.7484(1)	4.8314(1)	17.806(1)	−0.96(14)	3.4	10.65

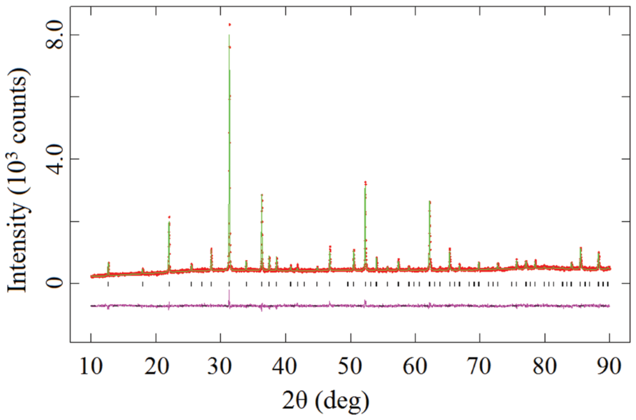

Fig. 2 Observed (red) and calculated (green) Cu K_α X-ray diffraction profiles of $Tb_2CoGe_4O_{12}$. A difference curve is also shown. Vertical markers indicate reflection positions.

moment of the Ln^{3+} cations in those compounds. These moments, listed in the last column of Table 1, are self-consistent and in excellent agreement with the predictions of the Landé formula. Although the intercation interactions are clearly weak above 150 K and $Ho_2CoGe_4O_{12}$ and $Er_2CoGe_4O_{12}$ are indeed paramagnetic throughout the measured temperature range, see Fig. 3, $Gd_2CoGe_4O_{12}$, $Tb_2CoGe_4O_{12}$, $Dy_2CoGe_4O_{12}$, $GdLuCoGe_4O_{12}$, $GdScCoGe_4O_{12}$, $TbScCoGe_4O_{12}$ and $DyScCoGe_4O_{12}$ all undergo a magnetic phase transition below 5 K, see Fig. 4. Below the temperature of the susceptibility maximum, some hysteresis is apparent between the ZFC and FC susceptibilities of $Tb_2CoGe_4O_{12}$, $Dy_2CoGe_4O_{12}$ and $DyScCoGe_4O_{12}$, but not between those the other compositions. The field dependence of the magnetisation of these six compositions at 2 K is included in Fig. 4, as is the temperature dependence of their ac susceptibility. The real and imaginary components of the latter are both frequency-dependent in the case of the two Dy-containing samples. No frequency dependence is apparent in the real part of the susceptibility of either $Tb_2CoGe_4O_{12}$ or $TbScCoGe_4O_{12}$ but a frequency-dependent imaginary component is clearly present in the former. In the case of the latter, only a very weak imaginary component is apparent below T_m, as is also the case for $Gd_2CoGe_4O_{12}$, $GdLuCoGe_4O_{12}$ and $GdScCoGe_4O_{12}$. In all cases $M(H)$ shows

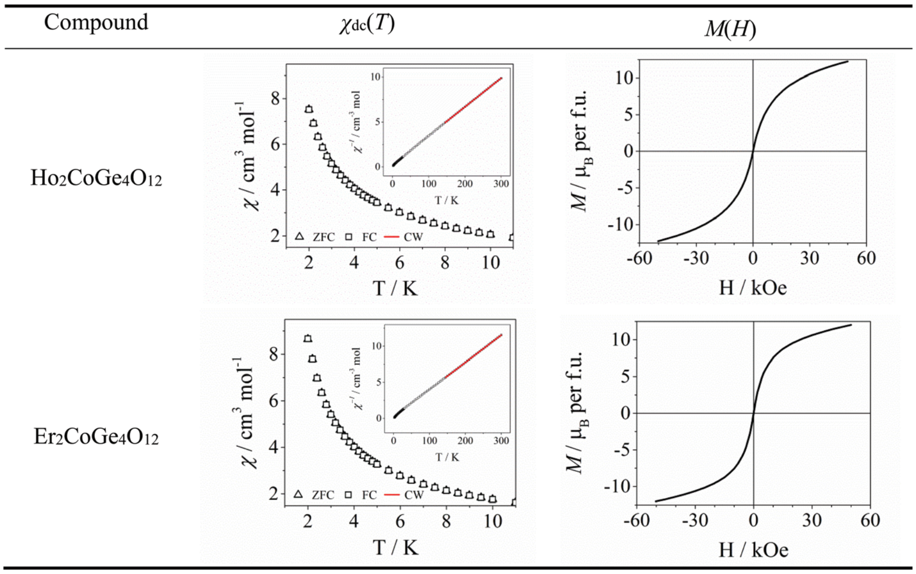

Fig. 3 Temperature dependence of the zero-field-cooled and field-cooled dc molar magnetic susceptibility and field-dependence of the magnetisation of $Ln_2CoGe_4O_{12}$ for Ln = Ho and Er. The red line shows a fit to the Curie–Weiss law.

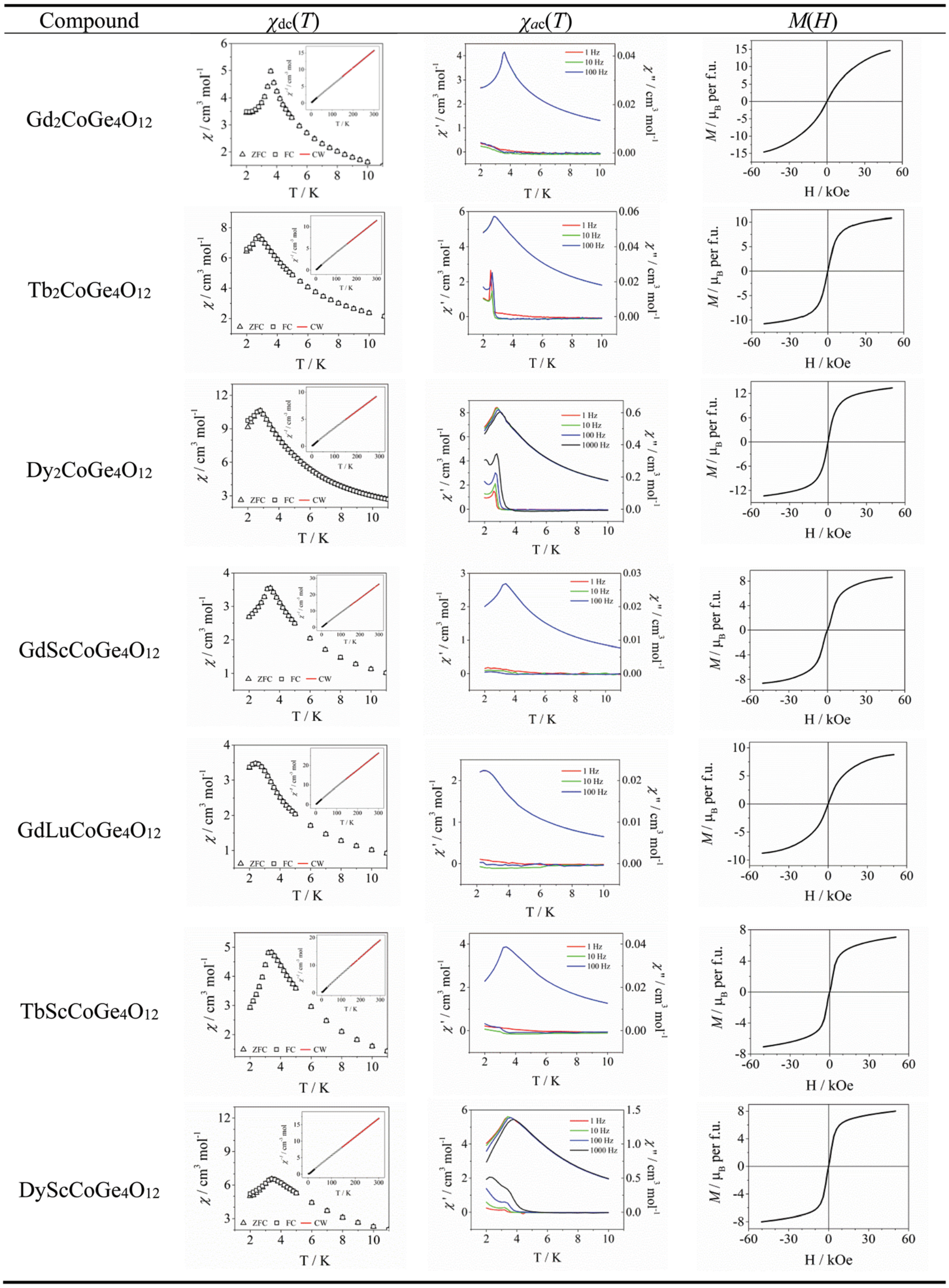

Fig. 4 Temperature dependence of dc and ac molar magnetic susceptibilities, χ, and field dependence of magnetisation per formula unit, $M(H)$, of $Ln_2CoGe_4O_{12}$ and $LnBGe_4O_{12}$.

the onset of saturation effects in relatively low fields. $\chi(H,T)$ is illustrated for selected compositions in Fig. 5. Note that if we set $k_BT = \mu_BH$ with $T = 4$ K, *i.e.* $\sim T_m$, then $H \sim 50$ kOe.

The ^{155}Gd Mössbauer spectra collected at 5 K are shown in Fig. 6. Where the gadolinium occurs on both the 2*b* and 4*f* sites ($Gd_2CoGe_4O_{12}$ and $GdLuCoGe_4O_{12}$), the spectra consist of two clearly distinct quadrupole doublets, whereas for $GdScCoGe_4O_{12}$, where the gadolinium occurs only on the 2*b* site, only a single quadrupole doublet is observed. The fitted parameters are given in Table 2. The inner doublet is assigned to gadolinium in the 2*b* site as it is the component that persists when only that site is occupied. The quadrupole moment of the $m_I = 5/2$ excited state is very small, so the paramagnetic spectrum is dominated by the splitting of the $m_I = 3/2$ ground state leading to an (almost) symmetric doublet and making it difficult to determine the sign of the electric field gradient

Compound	$\chi_{dc}(T)$
$Tb_2CoGe_4O_{12}$	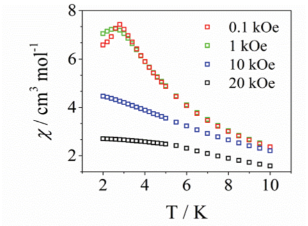
$Dy_2CoGe_4O_{12}$	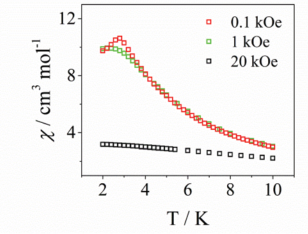
$TbScCoGe_4O_{12}$	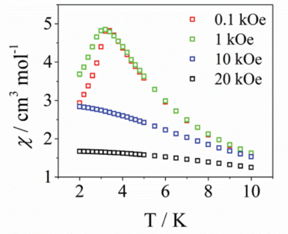
$DyScCoGe_4O_{12}$	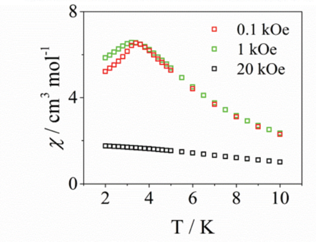

Fig. 5 Temperature and field dependence of the dc molar magnetic susceptibility of $Ln_2CoGe_4O_{12}$ and $LnBGe_4O_{12}$ for Ln = Tb, Dy; B = Sc.

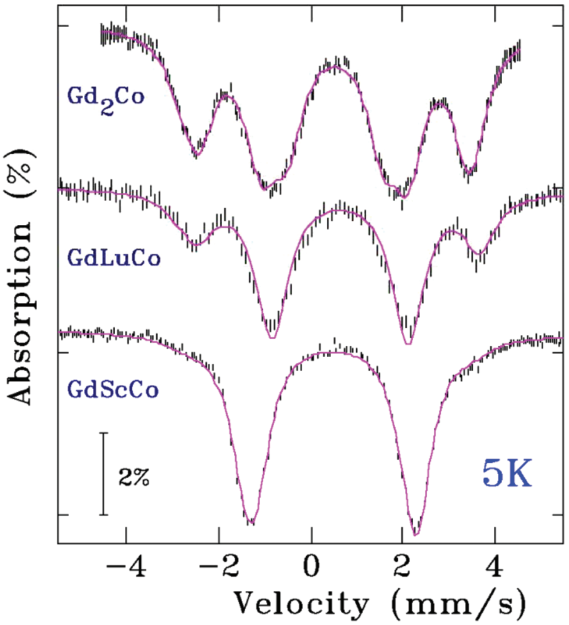

Fig. 6 Fits to the Mossbauer spectra collected from $Gd_2CoGe_4O_{12}$, $GdLuCoGe_4O_{12}$ and $GdScGe_4O_{12}$ at 5 K.

(efg). However, for the inner, stronger doublet in each case we observed a small but statistically significant asymmetry that allowed us to establish that the efg is positive at the 2*b* site. One striking feature of the spectra for $Gd_2CoGe_4O_{12}$ and $GdLuCoGe_4O_{12}$ is that the spectral areas of the components from the 2*b* and 4*f* sites are far from equal at 5 K, see Table 2. Our XRD data rule out the possibility of cobalt substituting for gadolinium on the 2*b* site and suggest that in both compositions the quantity of gadolinium on the 2*b* site is equal to that on the 4*f* site. The observed imbalance would then have to be due to differences in the recoil-free fractions at the two sites. Mössbauer spectroscopy relies on the recoil-free absorption of the gamma-ray in a nucleus in the sample. If the host atom is weakly bound, then a momentum-conserving recoil event is more likely and the Mössbauer signal is weaker. Where gadolinium occupies two crystallographically-distinct sites, the relative strength of the two signals is weighted not only by the frequency of occupation, but also by the probability of a zero-recoil event, set by the local binding strength. We therefore attribute the reduced area of the contribution from the 4*f* site to weaker binding of the gadolinium at this site. This explanation can be checked by raising the sample temperature, as increased thermal motion leads to a reduction in the recoil-free fraction (an effect that limits ^{155}Gd Mössbauer measurements to temperatures less than 60 K) and the reduction is more rapid if the host atom is more weakly bound. A check based on the isostructural compound $Gd_2MnGe_4O_{12}$ showed that the 2*b* : 4*f* ratio went from 60 : 40 at 5 K, to 70 : 30 at 60 K, fully consistent with weaker binding at the 4*f* site. We note that the ratio at 5 K is essentially the same for $Gd_2CoGe_4O_{12}$ and $Gd_2MnGe_4O_{12}$ but that the ratio for $GdLuCoGe_4O_{12}$ is significantly higher than both. We therefore propose that the 74 : 26 ratio observed in the lutetium-containing phase stems partly from a difference in the recoil-free fractions at the two sites but that it is also partly attributable to partial ordering of gadolinium and lutetium, with the larger gadolinium cations dominating on the eight-coordinate 2*b* sites. If we assume that the ratio of the recoil free fractions at 5 K is the same as in $Gd_2MnGe_4O_{12}$, then 65.5% of the gadolinium is on the 2*b* site, with the remaining 34.5% on the 4*f* site. This disorder was not detected in our XRD data because the two lanthanide elements have similar X-ray scattering lengths and our diffraction data were thus insensitive to the partial cation ordering. Cooling the samples to 1.8 K leads to magnetic ordering and the development of a magnetic hyperfine field (B_{hf}) at the gadolinium nuclei (see Fig. 7). The high point symmetry of the 2*b* site (422) provides some simplifying constraints as the efg tensor must be axially symmetric and the principal axis must be parallel to the crystallographic *c*-axis. No such constraints exist at the 4*f* site. The severe line overlap combined with the lack of independent constraints prevented us from developing a unique fit to the spectra of

Table 2 ^{155}Gd Mössbauer parameters at 5 K for $Gd_2CoGe_4O_{12}$ and $GdLuCoGe_4O_{12}$ and at 5 K and 1.8 K for $GdScCoGe_4O_{12}$

Composition	Temperature/K	Site	eQV_{zz}/mm s^{-1}	Area/%	B_{hf}/T	θ/°
$Gd_2CoGe_4O_{12}$	5	2*b*	5.58(3)	63(1)	—	—
		4*f*	12.67(2)	37(1)	—	—
$GdLuCoGe_4O_{12}$	5	2*b*	6.29(3)	74(1)	—	—
		4*f*	13.28(9)	26(1)	—	—
$GdScCoGe_4O_{12}$	5	2*b*	7.59(1)	100[a]	—	—
$GdScCoGe_4O_{12}$	1.8	2*b*	7.59(—)[b]	100[a]	24.7(2)	90

[a] Not refined. [b] Constrained to the value found at 5 K.

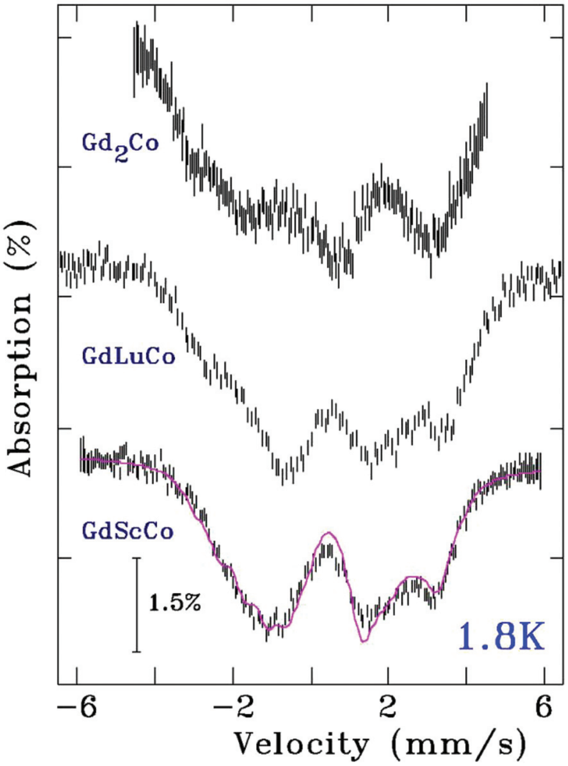

Fig. 7 Mossbauer spectra collected from $Gd_2CoGe_4O_{12}$, $GdLuCoGe_4O_{12}$ and $GdScCoGe_4O_{12}$ at 1.8 K. A fit to the spectrum of $GdScCoGe_4O_{12}$ is shown.

$Gd_2CoGe_4O_{12}$ and $GdLuCoGe_4O_{12}$ at 1.8 K, however the single site spectrum of $GdScCoGe_4O_{12}$ did admit analysis. The fit shown in Fig. 7 was obtained with the efg constrained to the value observed at 5 K. The main parameters that were varied to obtain the fit were B_{hf} and the angle, θ, between B_{hf} and the principal axis of the efg tensor (which we know to be parallel to the crystallographic *c*-axis). Our best fit gave $\theta = 90°$ indicating *ab*-plane ordering of the gadolinium moments. A free fit to θ yielded statistically equivalent fits with $\theta \sim 80°$ and $\theta \sim 100°$, reflecting the rather slow evolution in spectral shape near $\theta = 90°$. Within the precision of our measurements, the ordering of the gadolinium moments lies within the *ab*-plane.

The NPD patterns collected from $Tb_2CoGe_4O_{12}$ at room temperature using wavelengths of 1.622 and 2.4397 Å were consistent, see Fig. 8 and S1,† with the structural model described above. The structural parameters derived from a simultaneous analysis of both patterns are listed in Table 3 and the most important bond lengths and bond angles are listed in Table 4. The Tb^{3+} cations on the 2*b* sites are coordinated by eight equidistant O2 anions whereas the Tb/Co cations on the 4*f* sites are bonded to four O2 anions and two relatively-distant O1 anions. The GeO_4 tetrahedra contain equal numbers of O1 and O2 anions. A pattern collected at 5.5 K using a wavelength of 2.4397 Å could also be accounted for using the same model but additional Bragg peaks were apparent in a pattern collected at 1.5 K. These peaks occurred predominantly at low scattering angles and they were therefore assumed to be magnetic in origin. They could be accounted for, see Fig. 9, S1 and S2,† using the antiferromagnetic structure shown in Fig. 10. The magnetic unit cell is doubled along [001] compared to the structural unit cell. The cations lie in two antiferromagnetically-aligned (001) sheets at $z = \frac{1}{4}$ and $z = \frac{3}{4}$. Within each sheet the [100] components of the atomic moments on both the 2*b* and 4*f* sites are ferromagnetically aligned and the [010] components of nearest-neighbour cations on the 4*f* sites are antiferromagnetically coupled; no [010] component was found at the 2*b* sites. Simultaneous analysis of datasets collected at 1.5 K using neutron wavelengths of 1.622 and 2.4397 Å resulted in the atomic moments listed in Table 5. The struc-

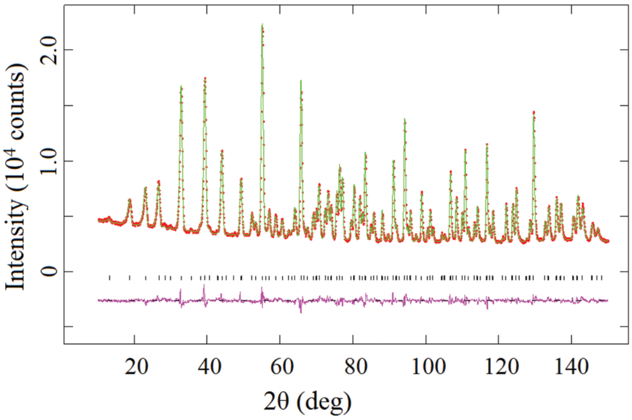

Fig. 8 Observed (red) and calculated (green) neutron diffraction profiles for $Tb_2CoGe_4O_{12}$ recorded using λ = 1.622 Å at 300 K; a difference curve is also shown. Vertical markers indicate reflection positions.

Table 3 Structural parameters of $TbBCoGe_4O_{12}$ (B = Tb or Sc) derived from neutron diffraction data at 300 and 1.5 K

		$Tb_2CoGe_4O_{12}$		$TbScCoGe_4O_{12}$	
		300 K	1.5 K	300 K	1.5 K
2*b* Tb/Sc[a]	$U_{iso}/Å^2$	0.0040(5)	0.0010(3)	0.0074(6)	0.0032(4)
4*f* Tb/Sc/Co[b]	$U_{iso}/Å^2$	0.0076(6)	0.0017(6)	0.0087(5)	0.0056(4)
8*k* Ge	x	0.5236(1)	0.5235(1)	0.5235(1)	0.5233(1)
	$U_{iso}/Å^2$	0.0064(2)	0.0036(2)	0.0047(2)	0.0058(2)
8*m* O1	x	−0.3694(1)	−0.3701(1)	−0.3692(1)	−0.3695(1)
	z	0.1686(2)	0.1700(2)	0.1796(2)	0.1797(2)
	$U_{iso}/Å^2$	0.0058(3)	0.0029(3)	0.0070(3)	0.0019(3)
16*n* O2	x	0.1682(1)	0.1683(1)	0.1623(1)	0.1621(1)
	y	0.0617(1)	0.0619(1)	0.0614(1)	0.0613(1)
	z	0.2559(2)	0.2552(2)	0.2559(2)	0.2568(2)
	$U_{iso}/Å^2$	0.0082(2)	0.0050(2)	0.0074(2)	0.0028(2)
a/Å		9.9039(1)	9.8975(1)	9.7799(1)	9.7785(1)
c/Å		4.9482(1)	4.9451(1)	4.8353(1)	4.8297(1)
$V/Å^3$		485.36(1)	484.42(1)	462.48(1)	461.82(1)
R_{wpr} [c]		3.26%	3.81%	3.56%	4.13%
R_{wpr} [d]		4.12%	4.57%	—	5.28%
χ^2		4.075	4.897	2.870	3.705

Space group *P*4/*nbm* (no. 125), *Z* = 2. 2*b* at $(\frac{1}{4}, \frac{1}{4}, \frac{1}{2})$; 4*f* at $(0, 0, \frac{1}{2})$; Ge on 8*k* $(x, \frac{1}{4}, 0)$; O1 on 8*m* $(x, -x, z)$; O2 on 16*n* (x, y, z). [a] Occupancy: 100% Tb for B = Tb; 86(1) % Tb, 0.14% Sc for B = Sc. [b] Occupancy: 50% Tb, 50% Co for B = Tb; 43% Sc, 7% Tb, 50% Co for B = Sc. [c] Derived from λ = 1.622 Å data. [d] Derived from λ = 2.4397 Å data.

Table 4 Bond lengths (Å) and bond angles (°) in $TbBCoGe_4O_{12}$ (B = Tb or Sc) derived from neutron diffraction data collected at 300 and 1.5 K

	$Tb_2CoGe_4O_{12}$		$TbScCoGe_4O_{12}$	
	300 K	1.5 K	300 K	1.5 K
2*b*-O2 × 8	2.365(1)	2.364(1)	2.351(1)	2.350(1)
4*f*-O1 × 2	2.456(1)	2.443(2)	2.382(2)	2.377(2)
4*f*-O2 × 4	2.147(1)	2.148(1)	2.068(1)	2.062(1)
O2–O2′ [a]	3.446(1)	3.439(2)	3.328(2)	3.319(1)
O2–O2″ [a]	3.068(2)	3.056(2)	3.969(2)	2.964(1)
Ge–O1 × 2	1.794(1)	1.797(1)	1.793(1)	1.794(1)
Ge–O2 × 2	1.724(1)	1.721(1)	1.720(1)	1.721(1)
O2–4*f*-O2′	96.72(3)	96.81(4)	96.59(3)	96.54(4)
O2–4*f*-O2″	83.28(3)	83.19(4)	83.41(3)	83.46(4)
O1–4*f*-O2′	82.81(3)	82.84(4)	83.07(4)	82.95(4)
O1–4*f*-O2″	96.72(3)	96.81(4)	96.59(4)	96.54(4)
O1–Ge–O1	107.58(9)	108.25(11)	108.36(10)	108.47(8)
O1–Ge–O2	104.93(4)	104.81(5)	104.95(5)	104.91(4)
O1–Ge–O2	108.74(6)	108.65(7)	107.91(6)	107.73(6)
O2–Ge–O2	121.33(7)	121.20(8)	122.21(9)	122.54(8)

[a] Distances within the equatorial plane of the oxide octahedra surrounding the 4*f* site.

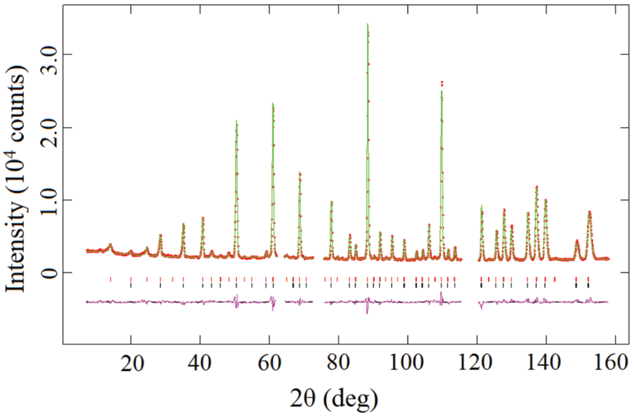

Fig. 9 Observed (red) and calculated (green) neutron diffraction profiles for $Tb_2CoGe_4O_{12}$ recorded using λ = 2.4397 Å at 1.5 K; a difference curve is also shown. Upper and lower vertical markers indicate magnetic and structural reflection positions, respectively.

tural parameters and agreement factors resulting from this analysis are listed in Table 3; the bond lengths are listed in Table 4. The magnetic space group is $P_{2c}b'an$ (#50.9.385, Opechowski-Guccione setting) and the magnetic propagation vector is $[0, 0, \frac{1}{2}]$.

Neutron diffraction data were collected on $TbScCoGe_4O_{12}$ at 300 K using a wavelength of 1.622 Å and at 1.5 K using both 1.622 and 2.4397 Å. Our initial refinements based on the assumption that Tb^{3+} occupies the 2*b* site with Sc^{3+} and Co^{2+} disordered over the 4*f* sites resulted in unphysical values for the displacement parameters at 1.5 K. We therefore reanalysed the data collected at 300 K, see Fig. 11, and established that Sc^{3+} and Tb^{3+} undergo significant site exchange, as represented by the formula $(Tb_{0.86(1)}Sc_{0.14})(Tb_{0.14}Sc_{0.86})CoGe_4O_{12}$. We also established that the fit to our X-ray diffraction data did not deteriorate significantly when this low level of disorder was included in the structural model. The site occupancies were held constant at these revised values during the analysis of the diffraction patterns collected at 1.5 K. Simultaneous analysis of the two datasets showed, see Fig. 12, S1 and S2,† that the magnetic structure was essentially the same as that of $Tb_2CoGe_4O_{12}$. The results of our study of $TbScCoGe_4O_{12}$ by neutron diffraction are included in Tables 3–5. The mean magnetic moment of 3.73μ_B per cation at the 2*b* site, see Table 5, corresponds to a moment of 4.32(6)μ_B per Tb^{3+} and the

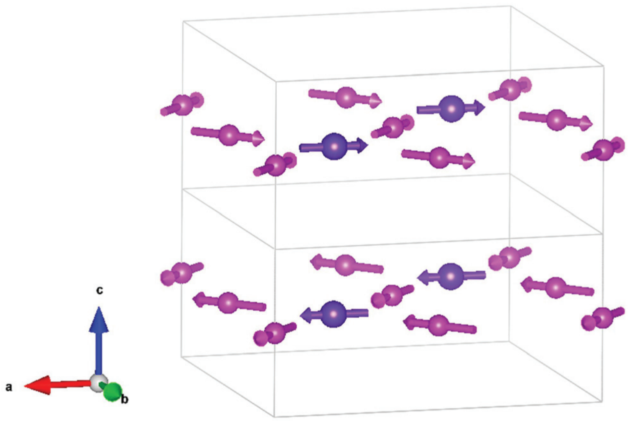

Fig. 10 Magnetic structure of $Tb_2CoGe_4O_{12}$. Cations on the 2*b* sites (Tb^{3+}) and 4*f* sites (Tb^{3+}/Co^{2+}) are shown in blue and purple, respectively.

Table 5 Atomic magnetic moments in $Tb_2CoGe_4O_{12}$ and $TbScCoGe_4O_{12}$ at 1.5 K

M	$Tb_2CoGe_4O_{12}$		$TbScCoGe_4O_{12}$	
	2*b* (Tb^{3+})	4*f* (Tb^{3+}/Co^{2+})	2*b* (Tb^{3+}/Sc^{3+})	4*f* ($Tb^{3+}/Sc^{3+}/Co^{2+}$)
M_x/μ_B	2.17(17)	0.89(9)	3.73(5)	1.23(3)
M_y/μ_B	—	0.98(11)	—	0.74(5)
M/μ_B	2.17(17)	1.32(14)	3.73(5)	1.44(5)

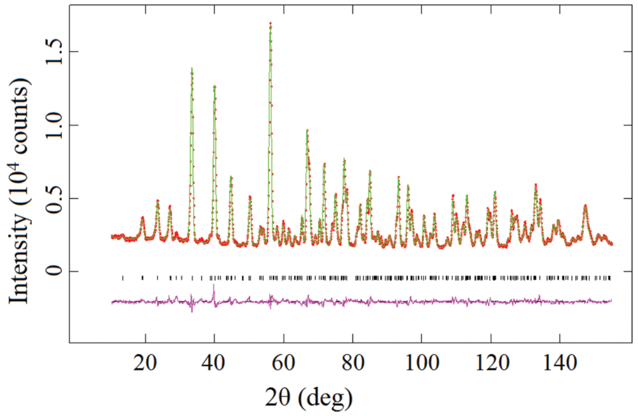

Fig. 11 Observed (red) and calculated (green) neutron diffraction profiles for $TbScCoGe_4O_{12}$ recorded using λ = 1.622 Å at 300 K; a difference curve is also shown. Vertical markers indicate reflection positions.

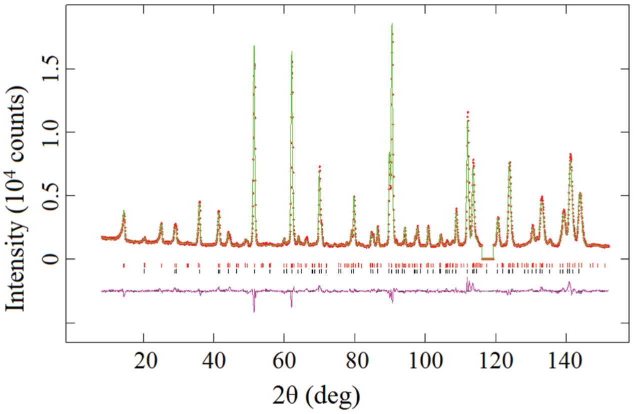

Fig. 12 Observed (red) and calculated (green) neutron diffraction profiles for $TbScCoGe_4O_{12}$ recorded using λ = 2.4397 Å at 1.5 K; a difference curve is also shown. Upper and lower vertical markers indicate magnetic and structural reflection positions, respectively.

moment of $1.44\mu_B$ per cation at the 4*f* site corresponds to a mean moment of $2.53(5)\mu_B$ per magnetic cation, averaged over 0.5 Co^{2+} and 0.07 Tb^{3+} cations. If we assume that the Tb^{3+} and Co^{2+} cations on the 4*f* site have the same ordered moments in $TbScCoGe_4O_{12}$ as in $Tb_2CoGe_4O_{12}$, then it follows that Tb^{3+} and Co^{2+} have moments of −0.2(1) and $2.9(1)\mu_B$, respectively. The moment on the Tb^{3+} cations is thus not significant compared to the standard deviation but, if present, it aligns anti-parallel to the direction the moment of a Co^{2+} cation would adopt on the same site. We note that the ordered moments of Co^{2+} in $ZrCo_2Ge_4O_{12}$ and $CeCo_2Ge_4O_{12}$ are 2.55(7) and 2.58(2) μ_B, respectively and that for a free Tb^{3+} cation $gJ = 9\mu_B$.

Discussion

The research described above constitutes a broad survey of the $Ln_2CoGe_4O_{12}$ family in which some compositions have been studied only briefly whereas others have been investigated in some detail. The compositions having Ln = Ho or Er received the least attention because the dc susceptibility data showed no evidence of a magnetic phase transition. Their susceptibility is dominated by the contribution from Ln and it is possible that any low-temperature decrease in susceptibility associated with an antiferromagnetic ordering of the Co^{2+} moments is masked by the continued increase of the contribution from Ln. However, our previous study of $Y_2CoGe_4O_{12}$ showed that the Co^{2+} ions that occupy half of the 4*f* sites cannot alone support long-range magnetic ordering and it is therefore likely that if the Ho^{3+} and Er^{3+} cations remain paramagnetic, then the Co^{2+} cations remain paramagnetic. The application of a 50 kOe magnetic field at 2 K results in an unsaturated magnetisation that is approximately equal to $g_{Ln}J_{Ln} + 2S_{Co}$, *i.e.* less than the value of $2g_{Ln}J_{Ln} + 2S_{Co}$ that might have been expected. Similarly reduced values have been observed previously in other compounds and attributed to either the presence of magnetic anisotropy in a powder sample or crystal field effects.[14–18]

We next consider the gadolinium-containing compositions. The dc susceptibility data suggest that $Gd_2CoGe_4O_{12}$, $GdScCoGe_4O_{12}$ and $GdLuCoGe_4O_{12}$, see Fig. 4, all order antiferromagnetically below 4 K in a field of 100 Oe, although the susceptibility maximum of $GdLuCoGe_4O_{12}$ is unusually broad. The absence of a paramagnetic contribution to the susceptibility below the transition temperature shows that all the magnetic cations are involved in the ordering. The temperature dependence of the ac susceptibilities is consistent with this conclusion, with only a very weak imaginary component being detected in each case. The Mössbauer spectra, see Fig. 7, confirm that the Gd^{3+} cations are magnetically ordered in each of the three compositions but quantitative analysis of the spectrum was only possible for $GdScCoGe_4O_{12}$ in which the Gd^{3+} cations are all located on the 2*b* site. The observation of magnetic order in this compound demonstrates the relative strength of the coupling between Co^{2+} on a 4*f* site and Gd^{3+} on a 2*b* site. This can be achieved *via* a Co–O2–Gd superexchange pathway, whereas such coupling between two 4*f* sites must involve a germanate group and is likely to be weaker. However, it is not clear that the ordering of the Ln moments in these compounds occurs by superexchange; dipolar interactions and the molecular field created by the ordered array of Co^{2+} moments might also play a part. The non-linear $M(H)$ behaviour of these compounds shows that fields in excess of ∼10 kOe start to overcome the antiferromagnetic coupling and in 50 kOe the magnetisation approaches the value predicted when Gd^{3+} and Co^{2+} are assigned moments of 7 and $3\mu_B$, respectively; unlike Ho^{3+} and Er^{3+}, isotropic Gd^{3+} ions with $L = 0$ are not susceptible to the effects of magnetic anisotropy and the crystal field.

There is no evidence in $\chi(T)$ for the presence of paramagnetic spins in $Dy_2CoGe_4O_{12}$ or $DyScCoGe_4O_{12}$ at the lowest temperature and the data suggest that they are spin glasses; the ZFC and FC dc susceptibilities are slightly different below the transition temperature and, more convincingly, the ac susceptibility is complex below a frequency-dependent transition temperature. The parameter $\Delta T_f/[T_f\Delta(\log\omega)]$ takes values of 0.024 and 0.039, respectively.[19] The imaginary component of the susceptibility in these two compounds is an order of magnitude stronger than that of $Tb_2CoGe_4O_{12}$ and two orders of magnitude stronger than those of the other compounds. However, the ratio θ/T_m, see Table 1, is unusually low for a spin glass. It can be seen, see Fig. 5, that the susceptibility is field-dependent below T_m in weak fields and over a wider temperature range in stronger fields; the transition broadens with increasing field strength. In the case of $Dy_2CoGe_4O_{12}$ the susceptibility decreases as the field is increased to 1 kOe whereas in the case of $DyScCoGe_4O_{12}$ an increase is observed. The former but not the latter could be attributed to saturation effects and we propose that both are actually caused by changes in the population of the m_J states of Dy^{3+}[14] that occur as a result of the superposition below T_m of an internal magnetic field on the pre-existing crystal field. The magnetic transition is not apparent in fields greater than or equal to 10 kOe and, as was the case for the compounds having Ln = Er or Ho, in a field of 50 kOe the magnetisation approaches values consistent with a contribution of $\sim 5\mu_B$ per Dy^{3+} cation, half of the value expected for a free ion. The formation of a spin-glass phase would imply that magnetic frustration is present and that not all of the pairwise intercation interactions can be satisfied simultaneously; the origin of this frustration is not clear at the present time It is possible that, as in $PbFe_{\frac{1}{2}}Nb_{\frac{1}{2}}O_3$,[20] the spin-glass phase coexists with a magnetically-ordered phase. Further work will be necessary before a complete description of these two compositions can be presented.

The present study focussed primarily on the two Tb^{3+}-containing compounds $Tb_2CoGe_4O_{12}$ and $TbScCoGe_4O_{12}$. The neutron diffraction data collected at room temperature did not reveal any anomalies in the structure of the former. The Tb^{3+} cations on the 2*b* sites are coordinated by eight equidistant oxide ions at the vertices of a square antiprism. The perpendicular distance between the two square faces of the antiprism is d_{pp} = 2.421(1) Å and the O2–O2 distance within a square face is d_{in} = 2.871(1) Å. The octahedron of oxide ions surrounding the Tb^{3+} cations occupying 4*f* sites is pseudo-tetragonal in that there are two equal Tb–O1 bonds *trans* to each other and four shorter Tb–O2 bonds that are almost perpendicular to the O1–Tb–O1 vector. However, the true point symmetry is monoclinic, see Table 4. Our refinements showed that in the case of $TbScCoGe_4O_{12}$ the scandium and terbium atoms are only ∼86% ordered over the 2*b* and 4*f* sites. This partial disorder can be contrasted with the situation in $GdScCoGe_4O_{12}$ where Mössbauer spectroscopy showed that the Gd^{3+} cations occupy only the 2*b* sites. Consideration of the relevant ionic radii[21] reveals that the 4*f* site in $Tb_2CoGe_4O_{12}$ is larger than is necessary to accommodate Tb^{3+} cations; the mean bond length around the site is 2.25 Å whereas the relevant radii sum to 2.184 Å. However, the Tb–O distance around the 2*b* site, 2.365 Å, is slightly shorter than the sum of the ionic radii, 2.39 Å. The Sc^{3+}/Tb^{3+} disorder in $TbScCoGe_4O_{12}$ thus relieves the strain at the 2*b* sites without inducing strain at the 4*f* sites. It is perhaps surprising that a similar degree of disorder does not occur in $GdScCoGe_4O_{12}$. In the absence of precise structural data on the latter composition we can only suggest that the changes that occur in order to accommodate the larger Gd^{3+} cations either eliminate the strain at the 2*b* site or remove the ability of the 4*f* site to accommodate an excess of Ln^{3+} cations. The perpendicular distance between the faces of the antiprism around the 2*b* site in $TbScCoGe_4O_{12}$ is d_{pp} = 2.349(1) Å and the O2–O2 distance is d_{in} = 2.879(1); the former is considerably shorter than the corresponding distance in $Tb_2CoGe_4O_{12}$ whereas the latter is essentially unchanged.

The dc susceptibility of $TbScCoGe_4O_{12}$ is characteristic of an antiferromagnet and the ac susceptibility shows only a very weak imaginary component, as was the case in $GdScCoGe_4O_{12}$. However, the susceptibility and the temperature width of the transition are a function of field, see Fig. 5, which is not the case in the majority of antiferromagnets. As in the case of $DyScCoGe_4O_{12}$, we suggest that the susceptibility increase observed when the field is increased from 0.1 to 1 kOe is a consequence of changes in the population of the m_J states of Ln^{3+} and the decrease observed in higher fields reflects a loss of antiferromagnetic ordering when $\mu_B H/k_B \sim T_m$, followed by the development of a saturated paramagnetic state. Fig. 4 shows that the high-field magnetisation is lower than might be expected if the anisotropic, $L = 3$ Tb^{3+} cations were acting as free ions and thus indicates that magnetic anisotropy and crystal field effects must again be taken into account. We shall

Table 6 Derived structural parameters for $Tb_2CoGe_4O_{12}$ and $TbScCoGe_4O_{12}$

Composition	$<r_{4f}>/r_{2b}$	$2c/a$	$d(M_{4f}\text{–O2})/d(M_{4f}\text{–O1})$	$\varphi/°$	$\psi/°$	d_{pp}/d_{in}
$Tb_2CoGe_4O_{12}$	0.802	0.9992	0.879(1)	81.60(8)	41.92(4)	0.843(1)
$TbScCoGe_4O_{12}$	0.745	0.9878	0.868(1)	81.42(8)	40.60(4)	0.816(1)

φ Angle between M_{4f}–O1 bond and M_{4f}–O2 bond. ψ Angle between the M_{4f}–O1 bond and the (001) plane.

return to this point below when we discuss the results of our neutron diffraction experiments. The behaviour of Tb_2CoGeO_4 is similar except that a small difference is apparent between the ZFC and FC dc susceptibilities below the transition temperature and, although the real part of the ac susceptibility is independent of frequency in the measured range, an imaginary component is clearly present. We do not currently have a satisfactory explanation for this observation. Before we embark on a detailed discussion of our low-temperature neutron diffraction data, we note that as the atomic number of Ln increases in this series of compounds there is apparently a progression from antiferromagnetism to spin-glass behaviour to paramagnetism. However, there is no systematic variation in the Weiss temperature, see Table 1. The increase in atomic number is accompanied by an increase in the orbital angular momentum, L and the spin–orbit coupling constant[22] and the concomitant change in the magnetic anisotropy is likely to be at least partly responsible for the changes in the nature of the magnetic ground state, perhaps through interplay between it and the crystal-field states of the different cations.

$Tb_2CoGe_4O_{12}$ and $TbScCoGe_4O_{12}$ adopt essentially the same magnetic structure at 1.5 K, see Fig. 12. Given the relationship $a = b \sim 2c$ that exists between the lattice constants of the structural unit cell, the ordered moments on the 4f sublattice can be described using the nomenclature devised by Wollan and Koehler[23] to describe spin ordering on a primitive cubic lattice. Thus the components of the moments along [100] order in an A-type manner and those along [010] order in a G-type manner. This spin arrangement also occurs in $CeCo_2Ge_4O_{12}$, but not in $ZrCo_2Ge_4O_{12}$. The factors that control the magnetic structure have been discussed in detail previously[8] and the parameters that were then considered to be important have been calculated for the two terbium-containing compounds, see Table 6. Comparison of these values with those in Table 5 of Xu *et al.*[8] would lead to the prediction that the doubling of the magnetic unit cell along [001] seen in $ZrCo_2Ge_4O_{12}$ will also occur in $TbScCoGe_4O_{12}$ but not in $Tb_2CoGe_4O_{12}$. The fact that the unit cell doubling does occur in the latter demonstrates that the introduction of the 4f electron system has a sufficiently large impact on the magnetic properties to invalidate the criteria developed previously. As discussed above, the moment per cation on the 4f site in $Tb_2CoGe_4O_{12}$ and $TbScCoGe_4O_{12}$ is compatible with Co^{2+} having a moment very similar to those observed previously in isostructural compounds, particularly if the Tb^{3+} cations are non-magnetic at low temperatures. It has previously been argued that crystal-field effects leave a Tb^{3+} cation on an octahedral site with a non-magnetic singlet ground state[24] and at the temperatures under discussion this ground state is likely to be achieved. The similarity in the behaviour of $Tb_2CoGe_4O_{12}$ and $TbScCoGe_4O_{12}$ is consistent with the presence in each case of a non-magnetic cation, Tb^{3+} or Sc^{3+}, on 50% of the 4f sites. The value of the refined moment at the 2b sites is in both cases significant but much lower than the free-ion value for Tb^{3+}. Fig. S2† illustrates the magnitude of the magnetic scattering that is attributable to Tb^{3+}. AlDamen *et al.*[14] have shown that the crystal field acting on Tb^{3+} in a trigonal prismatic environment also results in a non-magnetic ground state, although magnetic excited states can be thermally accessible even at low temperatures. We therefore propose that the moment measured on Tb^{3+} at the 2b site when $H = 0$, *i.e.* in a neutron diffraction experiment, might result from the population of low-lying excited states above a non-magnetic ground state. The separation of the different levels will be determined by the strength of the crystal field and the difference between the moments observed in our two terbium-containing compositions can thus be attributed to the differences in the Tb–O2 bond lengths and the interfacial distances, d_{pp}, in the two compounds. Alternatively, the internal magnetic field created by the ordered Co^{2+} cations might split the excited states such that a magnetic level becomes the ground state of the Tb^{3+} cations. The observation of effective magnetic moments of 9.68 and 9.97μ_B, see Table 1, in the temperature range $150 < T/K < 300$ shows that the crystal field splitting energies are negligible compare to k_BT in that temperature range. In both $Tb_2CoGe_4O_{12}$ and $TbScCoGe_4O_{12}$ the ordered moments of Tb^{3+} align parallel to the ferromagnetic, A-type component of the Co^{2+} spin structure in each (001) sheet. This arrangement could be adopted as a result of Co–O2–Tb superexchange, but dipolar coupling and the molecular field created by the Co^{2+} sublattice are also likely to play a role. Further work will be necessary in order to define definitively the origin of the coupling.

Conclusion

The isostructural compounds described above show a wide range of magnetic properties. Within the series $Ln_2CoGe_4O_{12}$ we have observed antiferromagnetism, spin-glass behaviour and paramagnetism. The first two phenomena are only observed below 4 K, *i.e.* in a temperature regime where the effect of the crystal-field on Ln^{3+} cations cannot be ignored. The observed behaviour has been attributed to the interplay of the crystal field, the magnetic anisotropy and the magnetic field, either external or internal. The antiferromagnetic spin structures adopted by $Tb_2CoGe_4O_{12}$ and $TbScCoGe_4O_{12}$ are essentially the same. This is consistent with the conclusion that in the case of the former the 4*f* site is occupied by Co^{2+} and Tb^{3+} cations rendered non-magnetic by the crystal field and in the case of the latter the site is occupied by Co^{2+}, diamagnetic scandium and a small concentration of non-magnetic Tb^{3+}; the same magnetic interactions are therefore present in both compounds. Mössbauer spectroscopy showed that the gadolinium-based compositions are also magnetically ordered at low temperatures. We did not collect neutron diffraction data on these strongly-absorbing compositions but we predict that, in view of the isotropic, $L = 0$ ground state of Gd^{3+}, the low-temperature spin structure of $Gd_2CoGe_4O_{12}$ will be different to that of $Tb_2CoGe_4O_{12}$. Additional complexity in the magnetic structure might be the cause of our failure to fit the Mössbauer spectrum collected at 1.8 K. However, we anticipate that the spin structure of $GdScCoGe_4O_{12}$ may be the same as that observed in the Tb^{3+}-containing compounds and our data analysis has established that the ordered moments lie in a plane perpendicular to [001] in each case.

Conflicts of interest

There are no conflicts to declare.

Acknowledgements

Financial support for this work was provided in part by the Natural Sciences and Engineering Research Council of Canada and the Fonds Québécois de la Recherche sur la Nature et les Technologies.

References

1 I. I. Leonidov, V. G. Zubkov, A. P. Tyutyunnik, N. V. Tarakina, L. L. Surat, O. V. Koryakova and E. G. Vovkotrub, *J. Alloys Compd.*, 2011, **509**, 1339–1346.

2 M. A. Melkozerova, N. V. Tarakina, L. G. Maksimova, A. P. Tyutyunnik, L. L. Surat, I. I. Leonidov, V. G. Zubkov, E. V. Zabolotskaya and R. F. Samigullina, *J. Sol-Gel Sci. Technol.*, 2011, **59**, 338.

3 N. V. Tarakina, V. G. Zubkov, I. I. Leonidov, A. P. Tyutyunnik, L. L. Surat, J. Hadermann and G. van Tendeloo, *Z. Kristallogr.*, 2009, 401–406.

4 V. G. Zubkov, N. V. Tarakina, I. I. Leonidov, A. P. Tyutyunnik, L. L. Surat, M. A. Melkozerova, E. V. Zabolotskaya and D. G. Kellerman, *J. Solid State Chem.*, 2010, **183**, 1186–1193.

5 D. Xu, M. Sale, M. Avdeev, C. D. Ling and P. D. Battle, *Dalton Trans.*, 2017, **46**, 6921–6933.

6 X.-Q. Liu, P. D. Battle, J. Ridout, D. Xu and S. Ramos, *J. Solid State Chem.*, 2015, **228**, 183–188.

7 D. Xu, M. Avdeev, P. D. Battle and X. Q. Liu, *Inorg. Chem.*, 2017, **56**, 2750–2762.

8 D. Xu, M. Avdeev, P. D. Battle, J. M. Cadogan and H. Lamont, *J. Solid State Chem.*, 2017, **254**, 40–46.

9 H. M. Rietveld, *J. Appl. Crystallogr.*, 1969, **2**, 65–71.

10 A. C. Larson and R. B. von-Dreele, *General Structure Analysis System (GSAS), Report LAUR 86-748*, Los Alamos National Laboratories, 1994.

11 B. H. Toby, *J. Appl. Crystallogr.*, 2001, **34**, 210–213.

12 B. van Laar and W. B. Yelon, *J. Appl. Crystallogr.*, 1984, **17**, 47–54.

13 C. J. Voyer and D. H. Ryan, *Hyperfine Interact.*, 2006, **170**, 91–104.

14 M. A. AlDamen, S. Cardona-Serra, J. M. Clemente-Juan, E. Coronado, A. Gaita-Arino, C. Marti-Gastaldo, F. Luis and O. Montero, *Inorg. Chem.*, 2009, **48**, 3467–3479.

15 S. T. Bramwell, M. N. Field, M. J. Harris and I. P. Parkin, *J. Phys.: Condens. Matter*, 2000, **12**, 483–495.

16 A. M. Hallas, J. A. M. Paddison, H. J. Silverstein, A. L. Goodwin, J. R. Stewart, A. R. Wildes, J. G. Cheng, J. S. Zhou, J. B. Goodenough, E. S. Choi, G. Ehlers, J. S. Gardner, C. R. Wiebe and H. D. Zhou, *Phys. Rev. B: Condens. Matter*, 2012, **86**, 134431.

17 X. Ke, M. L. Dahlberg, E. Morosan, J. A. Fleitman, R. J. Cava and P. Schiffer, *Phys. Rev. B: Condens. Matter*, 2008, **78**, 104411.

18 E. Morosan, J. A. Fleitman, Q. Huang, J. W. Lynn, Y. Chen, X. Ke, M. L. Dahlberg, P. Schiffer, C. R. Craley and R. J. Cava, *Phys. Rev. B: Condens. Matter*, 2008, **77**, 224423.

19 J. A. Mydosh, *Spin glasses: an experimental introduction*, Taylor & Francis, London, 1993.

20 S. Chillal, M. Thede, F. J. Litterst, S. N. Gvasaliya, T. A. Shaplygina, S. G. Lushnikov and A. Zheludev, *Phys. Rev. B: Condens. Matter*, 2013, **87**, 220403.

21 R. D. Shannon, *Acta Crystallogr., Sect. A: Cryst. Phys., Diffr., Theor. Gen. Cryst.*, 1976, **32**, 751–767.

22 D. Aravena, M. Atanasov and F. Neese, *Inorg. Chem.*, 2016, **55**, 4457–4469.

23 E. O. Wollan and W. C. Koehler, *Phys. Rev.*, 1955, **100**, 545–563.

24 B. R. Cooper and O. Vogt, *Phys. Rev. B: Solid State*, 1970, **1**, 1218–1226.